Journal of the Korean Society of Surveying, Geodesy, Photogrammetry and Cartography
Vol. 33, No. 3, 211-218, 2015
http://dx.doi.org/10.7848/ksgpc.2015.33.3.211

ISSN 1598-4850(Print)
ISSN 2288-260X(Online)
Original article

Automatic Cross-calibration of Multispectral Imagery with Airborne Hyperspectral Imagery Using Spectral Mixture Analysis

Kim, Yeji[1] · Choi, Jaewan[2] · Chang, Anjin[3] · Kim, Yongil[4]

Abstract

The analysis of remote sensing data depends on sensor specifications that provide accurate and consistent measurements. However, it is not easy to establish confidence and consistency in data that are analyzed by different sensors using various radiometric scales. For this reason, the cross-calibration method is used to calibrate remote sensing data with reference image data. In this study, we used an airborne hyperspectral image in order to calibrate a multispectral image. We presented an automatic cross-calibration method to calibrate a multispectral image using hyperspectral data and spectral mixture analysis. The spectral characteristics of the multispectral image were adjusted by linear regression analysis. Optimal endmember sets between two images were estimated by spectral mixture analysis for the linear regression analysis, and bands of hyperspectral image were aggregated based on the spectral response function of the two images. The results were evaluated by comparing the Root Mean Square Error (RMSE), the Spectral Angle Mapper (SAM), and average percentage differences. The results of this study showed that the proposed method corrected the spectral information in the multispectral data by using hyperspectral data, and its performance was similar to the manual cross-calibration. The proposed method demonstrated the possibility of automatic cross-calibration based on spectral mixture analysis.

Keywords : Cross-calibration, Spectral Mixture Analysis, Spectral Unmixing, Hyperspectral Image, Multispectral Image

1. Introduction

As the number of Earth observation satellites has increased, an increasing amount of remote sensing data has been extended to applications of remote sensing in different fields of study. Remote sensing data acquired from multiple sensors at various acquisition times have been used for continuous data collection within a given time to increase the accuracy of analysis. Because result of remote sensing analysis depends on accurate data and consistent measurement over a given period, remote sensing data gathered from various imaging sensors and under different atmospheric conditions must be on a consistent radiometric scale. Radiometric calibration for the consistent radiometric scale can be conducted through the ground prior to launch, onboard the spacecraft post-launch, and cross-calibration based on reference images of the Earth. Among these methods, cross-calibration is the feasible solution to place both similar and different sensors on a common radiometric scale without the need of field data or sensor information. Hence, cross-calibration could play an important role in interoperability and data fusion (Chander *et al*., 2013).

Received 2015. 06. 11, Revised 2015. 06. 19, Accepted 2015. 06. 29
1) Member, Department of Civil and Environmental Engineering, Seoul National University (Email: yjkimjl@snu.ac.kr)
2) Member, School of Civil Engineering, Chungbuk National University (Email: jaewanchoi@chungbuk.ac.kr)
3) Member, Civil Engineering, Texas A&M University-Corpus Christi (Email: Anjin.Chang@tamucc.edu)
4) Corresponding Author, Member, Department of Civil and Environmental Engineering, Seoul National University (E-mail: yik@snu.ac.kr)

Several previous studies performed cross–calibration techniques on multispectral images, such as Landsat TM and ETM. Song (2004) proposed a simple approach to cross-sensor calibration for NDVI indices. In their study, IKONOS and Landsat ETM+ were divided into vegetation and non-vegetation areas by the segmentation and classification of an IKONOS image. The NDVI values in each area were calibrated by histogram matching. Röder *et al*. (2005) developed the radiometric inter-calibration of Landsat TM and MSS, which was used to perform the normalization of radiometrically uncorrected images using the available knowledge of parameters for the radiometrically corrected image. Teillet *et al*. (2007) investigated Spectral Band Difference Effects (SBDE), which are significant in cross-calibration between multiple satellite sensors. They also demonstrated cross-calibration requires that the spectral dependencies of the sensor responses and scene illumination, atmosphere, and surface were taken into account. On the other hand, Brook and Dor (2011) used vicarious calibration targets to correct sensor radiance within a short period. Chander *et al*. (2013) introduced the Spectral Band Adjustment Factor (SBAF), which determines the spectral profile of the target and relative spectral responses between Landsat ETM+ and MODIS images. This study used additional Hyperion data to derive the spectral signature of the target for SBAF computation.

As Chander *et al*. (2013) presented on their study, hyperspectral images with narrow spectral band range is a good reference data for radiometric calibration of remote sensing data collected by multi-sensors, when the hyperspectral images are radiometrically corrected. For the effective analysis of precise spectral information in hyperspectral images, spectral unmixing or spectral mixture analysis, has been developed for its use in various applications to hyperspectral images (Heinz and Chang, 2001; Franke *et al*., 2009; Raksuntorn and Du, 2010). Spectral unmixing is the procedure by which the measured spectrum of a mixed pixel is decomposed into a collection of constituent spectra, or endmembers, and a set of corresponding fractions, or abundances, that indicate the proportions of each endmember present in the pixel (Keshava, 2003). Many previous studies on spectral unmixing applied nonnegative matrix factorization (NMF) for remote sensing analysis. Since Paatero and Tapper (1994) and Lee and Seung (1999) introduced the NMF, it has become well known as effective in finding reduced rank nonnegative factors to approximate a given nonnegative data matrix (Berry *et al*., 2007). Based on NMF, Yokoya *et al*. (2013) introduced Coupled NMF (CNMF) to fuse the hyperspectral and multispectral images collected from the same sensor. This technique was used to optimize the abundance maps of multispectral images and the endmembers of hyperspectral images by unmixing NMF iteratively so that the fused images resulted intermediate spectral information on similarities and differences between the multispectral and hyperspectral images.

Using hyperspectral data and spectral mixture analysis technique, we present an automatic cross-calibration method to calibrate the multispectral image used in this study. The spectral characteristics of the multispectral image were adjusted using linear regression analysis based on the endmember sets from two images, which were automatically extracted using spectral unmixing techniques. The bands in the hyperspectral image were aggregated based on the spectral response function to reduce the difference in relative spectral responses between the spectral bands of two images.

2. Methodology

The method proposed for the cross-calibration of hyperspectral images is divided into three parts. The first section includes the conversion to Top of Atmosphere (TOA) and histogram matching to reference the data and determine the target data. These data need to be calibrated before performing spectral unmixing between the reference data and the target data. The second section is the endmember set estimation. The endmember set estimation between the hyperspectral and multispectral images is performed using NMF based on the spectral unmixing approach. In spectral unmixing, the linear model is generally recognized as acceptable in many real-world scenarios even though it is not always true, such as in collected conditions with strong non-linearity (Keshava, 2003). Both hyperspectral

images, which are reference image (*REF*) and multispectral images, which are target data (*TAR*), can be unmixed into endmember and abundance as follows:

$$REF = em_{REF} \times abun_{REF} + \upsilon \quad (1)$$

$$TAR = em_{TAR} \times abun_{TAR} + \upsilon \quad (2)$$

In Eq. (1), *REF* is a hyperspectral image, υ represents noise, and em_{REF} and $abun_{REF}$ are endmember spectrum collection and their abundance map of *REF*, respectively. In Eq. (2), *TAR* is a multispectral image that needs to be calibrated, em_{TAR} and $abun_{TAR}$ are endmember sets and their abundance map of *TAR*, respectively. To estimate *gain* and *offset* through linear regression analysis, em_{REF} and em_{TAR} require the spectral information about identical materials on the scene. Because it is difficult to estimate em_{REF} and em_{TAR} in the same material directly from Eqs. (1) and (2), we adopted CNMF to calculate the optimized em_{REF} and em_{TAR} between *REF* and *TAR* (Yokoya *et al*., 2012). The origianl CNMF is focused on the image fusion of images collected simultaneously from same sensor system and estimates endmember sets and abundance maps assuming that the images have less atmospheric and radiometric differences (Yokoya *et al*., 2012). Because the concept of cross-calibration is to calibrate images radiometrically and atmospherically by using a radiometric- and atmospheric-corrected image, we focused to estimate endmember sets between images although the images have high atmospheric and radiometric differences.

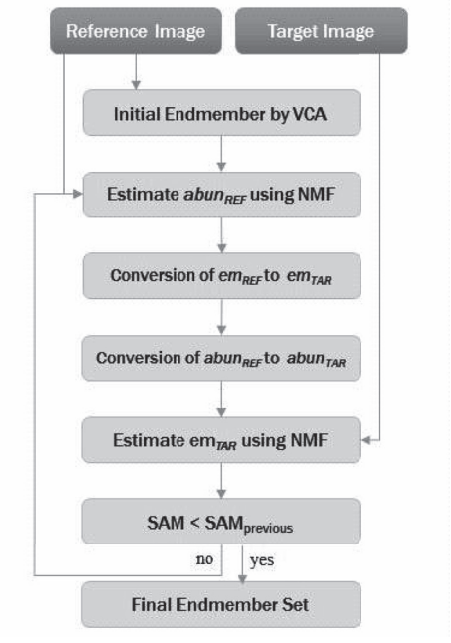

Fig. 1. Process of the endmember set estimation

Fig. 1 shows the entire process of the endmember set estimation that we proposed. Each NMF unmixing updates the endmember sets or abundance maps of *REF* and *TAR*, which was done using multiplicative update rules as follows:

$$em^{i+1} = em^{i} \times \frac{(IMG \times abun^{T})}{em^{i} \times (abun \times abun^{T})} \quad (3)$$

$$abun^{i+1} = abun^{i} \times \frac{(em^{T} \times IMG)}{em^{T} \times (em \times abun^{i})} \quad (4)$$

In Eqs. (3) and (4), *em* is either em_{REF} or em_{TAR}, and *abun* is either $abun_{REF}$ or $abun_{TAR}$. *IMG* represents *REF* or *TAR* in each step. $abun^{T}$ and em^{T} denote the transposition of a matrix *abun* and *em*, respectively. em^{i} and $abun^{i}$ are the *em* and *abun* in *i*th iteration step and can be updated to em^{i+1} and $abun^{i+1}$ using Eqs. (3) and (4) (Berry *et al*., 2007).

The initial endmember set of *REF* for the first NMF unmixing was estimated using vertex component analysis (VCA), which is an endmember extraction algorithm known for its fast processing in estimating the endmember spectrum in hyperspectral images (Nascimento and Bioucas-Dias, 2005). The initial ratio in each pixel of $abun_{REF}$ was 1 divided by the total number of endmembers. Eq. (4) was used with *REF* as *IMG* and $abun_{REF}$ as *abun* to estimate $abun_{REF}$ first. Then em_{REF} and the estimated $abun_{REF}$ were updated by Eqs. (3) and (4) where *REF* is *IMG*. The updated em_{REF} was converted to em_{TAR} by multiplying the spectral response function matrix between *REF* and *TAR* (BlackBridge, 2012). The updated $abun_{REF}$ was also converted to $abun_{TAR}$ by applying the point spread function by considering the spatial resolution of *REF* and *TAR* (Yokoya *et al*., 2012; Chi, 2013). The second NMF unmixing was performed using the converted em_{TAR} and $abun_{TAR}$. At this time, em_{TAR} was updated by Eq. (3), where *TAR* was *IMG* and $abun_{TAR}$ is *abun* first. Then em_{TAR} and the estimated $abun_{TAR}$ were updated by Eqs. (3) and (4), where *REF* is *IMG*. After the first and second NMF unmixing, the SAM value was estimated to measure

the similarity of the updated em_{REF} and em_{TAR}. Because the SAM is insensitive to variations in illumination, it is effective to estimate the similarity of the updated em_{REF} and em_{TAR} from images collected with different radiometric and atmospheric conditions. It uses the vector direction rather than the vector length. SAM becomes closer to zero as two images become spectrally similar. It can be calculated by Eqs. (5), where $V_{result1}$ denotes the generic pixel vector element of the previous result and $V_{result2}$ denotes the generic pixel vector element of the updated result. (Stathaki, 2008).

$$SAM = \arccos\left(\frac{\langle V_{result1}, V_{result2}\rangle}{\| V_{result1} \| \cdot \| V_{result2} \|}\right) \quad (5)$$

The second iteration process was performed by re-starting the first NMF unmixing with the updated em_{REF}, not the initial em_{REF} estimated by VCA. The SAM value between the updated em_{REF} and em_{TAR} determined from the second iteration process. This was compared with the SAM value estimated in the first iteration process. If the current SAM value was smaller than the previous SAM value or the iteration loop reached a maximum number of iterations, the iteration loop was ended.

After the optimal endmember set between *REF* and *TAR* was estimated, band aggregation was performed based on the spectral response function of *REF* and *TAR*. Using em_{REF} after the band aggregation and em_{TAR} from the optimal endmember set, we performed linear regression analysis and calibrated the *TAR* by applying estimated *gain* and *offset* to get calibrated result, $TAR_{calibrated}$, as follow:

$$TAR_{calibrated} = (gain \times TAR) + offset \quad (6)$$

3. Study Site and Data

The hyperspectral images collected by the airborne CASI-1500 sensor were used to calibrate RapidEye multispectral images. The CASI-1500 sensor was developed by ITRES Research Ltd. of Canada. This sensor is a pushbroom imaging spectrometer with a spectrum ranging from 380 nm to 1050 nm. The CASI images used in this study were taken in the Sejong-bo area in Sejong-Ri Yeongi-Myun Sejong-Si, Korea on 2 May 2014. Radiometric calibration, geometric correction, and optional environmental calibration were applied to collected stripes of CASI images to obtain orthocorrected images. RapidEye is a German geospatial information provider that operates five observation satellites. It is the first commercial sensor to detect the Red Edge band and provides data with a spatial resolution of 5 m GSD at nadir. The RapidEye scene for this study was collected at Sejong-si, including Sejong-bo, on 1 May 2014. The product level was 1B, which is radiometric- and sensor-corrected and provides imagery as seen from the spacecraft without correction for any geometric distortions inherent in the imaging process. The specifications of the CASI and RapidEye images and the site scene are presented in Table 1, Fig. 2, and Fig. 3.

Table 1. Specifications of CASI and RapidEye images

Sensors	CASI-1500	RapidEye	
Spatial Resolution (GSD)	1 m	5 m	
Spectral Resolution (nm)	48 Bands (363-1052)	Blue	440-510
		Green	520-590
		Red	690-730
		Red Edge	630-685
		NIR	760-850
Acquisition Date	2014/05/02	2014/05/01	

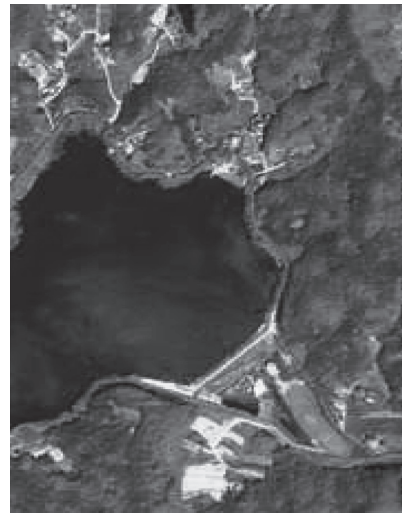

Fig. 2. Study site 1 displayed in 858.5 nm, 643.3 nm, and 557.2 nm as RGB channel

Fig. 3. Study site 2 displayed in 858.5 nm, 643.3 nm, and 557.2 nm as RGB channel

Registration between the CASI and RapidEye images was performed with manually collected GCPs. Study sites 1 and 2 were selected from areas that included water, vegetation, paddy fields, and urban structures.

In this study, the number of endmembers was set at 30. The maximum number of iterations of the entire loop was five because high numbers of the iteration of the entire loop caused abnormal abundance fractions because of the radiometric difference between the CASI and RapidEye images. The maximum number of iterations in individual NMF unmixing was set at 300 for optimal updating and appropriate time expenses. The threshold value to exit the individual NMF unmixing iteration by using Frobenius norm was set at 0.0001 (Yokoya *et al*., 2012).

The results of the proposed cross-calibration method were compared with the results of empirical line calibration (ELC) utility in an ENVI program, which performed the cross-calibration with manually collected regions of interest (ROIs); 30 ROIs from the scene were collected manually from invariant features of urban structure, water, forest, paddy fields, and more to process the empirical line calibration. Both results were statically evaluated using the root mean square error (RMSE) and SAM to compare the pixel difference and spectral difference in the calibrated results with the reference data. The RMSE and SAM values were calculated using Eqs. (7) and (5), respectively. In Eq. (7), *n* is the total number of pixel, and *reference* (*i*) and *result* (*i*) are the reflectance value of *i*th pixel in reference and result images, respectively. In Eq. (5), *result 1* is reference and *result 2* is the calibration result image. The average percent difference was also calculated to compare differences before and after cross-calibration. The average percent difference indicates the degree in percentage of the differences between the pixels in two images. It was calculated by Eq. (8), where *reference* is the matrix with reflectance values of reference and *result* is the matrix with reflectance values of calibration result (Chander *et al*., 2013).

$$RMSE = \sqrt{\frac{\sum_{i=1}^{n}(reference(i) - result(i))^2}{n}} \tag{7}$$

$$average\ \%\ difference = \frac{reference - result}{result} \tag{8}$$

4. Result and Discussion

Table 2 presents the results of the statistical evaluation of the cross-calibration of the RapidEye image using the CASI image. The RMSE and SAM indices of the results of ELC and the proposed method were calculated using CASI data and RapidEye-ATCOR data as references. The similarity of the spectral information in the cross-calibration results was evaluated by comparing with the CASI data. RapidEye-ATCOR is an atmospherically corrected version of RapidEye data in reflectance by using ATCOR. It was used as a reference to evaluate the effectiveness of the proposed method as an atmospheric correction tool. The RMSE and SAM indices in Table 3 show the spectral differences in the cross-calibration results compared to CASI and RapidEye-ATCOR. The results of the ELC showed higher RMSE and SAM values than the results of the proposed method did, comparing to the CASI image and RapieEye-ATCOR. The RMSE and SAM indices demonstrate that the results of the proposed method showed fewer spectral variations and fewer differences of reflectance values in the CASI image. The RMSE of the proposed method was increased in study site 2

while that of ELC was decreased, comparing to the results of study site 1. It could be caused by lower variety of extracted endmembers for proposed method because study site 2 had urban structures with high spectral diversity and abnormal reflectance values comparing to study site 1.

Table 2. Comparison of RMSE and SAM indices for cross-calibration results

Compared with		CASI		RapidEye-ATCOR	
Methods		ELC	Proposed Method	ELC	Proposed Method
Site 1	RMSE (ideal = 0)	437.378	235.920	1350.090	1277.202
	SAM (ideal = 0)	0.484	0.393	0.587	0.295
Site 2	RMSE (ideal = 0)	326.397	274.006	1416.232	1568.511
	SAM (ideal = 0)	0.194	0.198	0.208	0.208

Table 3 presents the average percentage differences between the results and the CASI image before and after cross-calibration, which were used to evaluate the differences in the pixel values before and after calibration. Before the cross-calibration, the average percentage difference between the CASI and original RapidEye images of study site 1 was –0.883%. After the cross-calibration, the average percentage difference between the CASI image and the ELC result was reduced to –0.478%. The average percentage difference between the CASI image and the results of the proposed method was greatly reduced to 0.045%. In study site 2, the average percentage difference was –0.833% before the calibration, but it increased to –0.053% and 0.069% after cross-calibration, using the ELC and the proposed method, respectively. As the SAM values on site 1, the higher value of the average percentage difference in the result of the proposed method for study site 2 could be caused by the spectral diversity and abnormality of urban structures on study site 2. The high spectral diversity and abnormal reflectance values could interrupt to extract endmembers of main components on study site 1, although the components that mainly cover the study site needed to be extracted as endmembers for the efficient cross-calibration. Since the difference of the lower SAM values and the higher average percentage difference value was not relatively high, the cross-calibration results of the proposed method and ELC had similar quality on study site 2.

Table 3. Average % difference before and after cross-calibration

Compared with		CASI	
Methods		ELC	Proposed Method
Site 1	Average % difference before calibration (%)	-0.883	
	Average % difference after calibration (%)	-0.478	0.045
Site 2	Average % difference before calibration (%)	-0.833	
	Average % difference after calibration (%)	-0.053	0.069

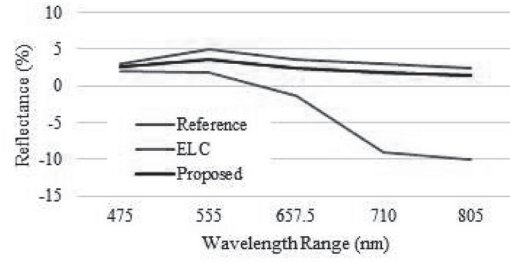

(a)

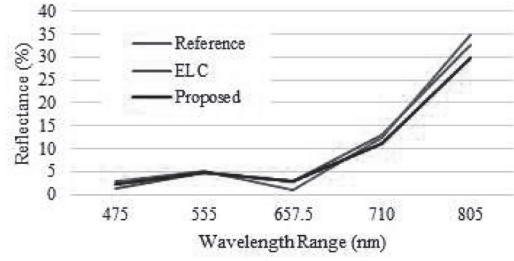

(b)

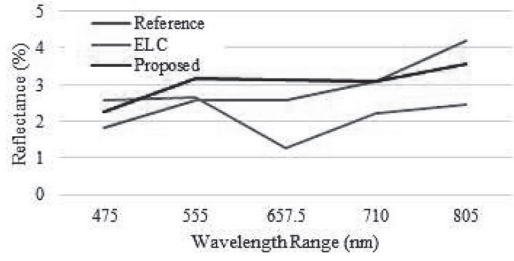

(c)

Fig. 4. Comparison of spectral graphs (a) at lake on study site 1, (b) at forest on study site 2, and (c) at shading net in ginseng fields on study site 2

Fig. 4 displays the spectral graphs of the pixels in three different materials in the study sites. The proposed result of water pixel displayed in Fig. 4 (a) has higher spectral similarity than the ELC result. The forest pixel in study site 2 demonstrated that the proposed calibration method corrected the spectral information in the RapidEye data closer to CASI data than the ELC did. At the shading net in ginseng fields, both the spectral information in ELC and the proposed method were close to the CASI data.

5. Conclusion

In this study, we introduced the cross-calibration of a multispectral image using a hyperspectral image. Based on the spectral unmixing technique, the proposed method selected endmember sets from multispectral and hyperspectral images to estimate the optimized endmember sets automatically for identical materials on land. The results showed that the proposed method corrected the spectral variations in the multispectral image based on the hyperspectral image as much as the manual calibration of ELC did. Some results showed that the radiometric corrections performed by the proposed method were better than those performed by the ELC. The proposed method demonstrated the possibility of automatic cross-calibration between simultaneous remote sensing images. Automatic cross-calibration could save time without the need for manual input, such as in the selection of ROIs and the collection of ground data. The proposed method allows for the simple and easy radiometric calibration of remote sensing data if a reference image is available. Furthermore, this method could be developed for the radiometric correction of remote sensing data collection for time series analysis.

Acknowledgment

This work was supported by the Space Core Technology Development Program through the National Research Foundation of Korea (NRF) and funded by the Ministry of Science, ICT & Future Planning (NRF-2012M1A3A3A02033469).

References

Berry, M.W., Browne, M., Langville, A.N., Pauca, V.P., and Plemmons, R.J. (2007), Algorithms and applications for approximate nonnegative matrix factorization, *Computational Statistics and Data Analysis*, Vol. 52, No. 1, pp. 155-173.

BlackBridge (2012), Spectral response curves of the RapidEye sensor, *BlackBridge*, German, http://blackbridge.com/rapideye/upload/Spectral_Response_Curves.pdf (last date accessed: 8 June 2015).

Brook, A. and Dor, E.B. (2011), Supervised vicarious calibration (SVC) of hyperspectral remote-sensing data, *Remote Sensing of Environment*, Vol. 115, No. 6, 1543-1555.

Chander, G., Mishra, N., Helder, D.L. Aaron, D.B., Angal, A., Choi, T., Xiong, X., and Doelling, D.R. (2013), Applications of spectral band adjustment factors (SBAF) for cross-calibration, *IEEE Transactions on Geoscience and Remote Sensing*, Vol. 51, No. 3, 1267-1281.

Chi, J. (2013), Validation of the radiometric characteristics of Landsat 8 (LDCM) OLI Sensor using band aggregation technique of EO-1 Hyperion hyperspectral imagery, *Korean Journal of Remote Sensing*, Vol. 29, No. 4, pp. 399-406. (in Korean with English abstract)

Franke, J., Roberts, D.A., Halligan, K., and Menz, G. (2009), Hierarchical multiple endmember spectral mixture analysis (MESMA) of hyperspectral imagery for urban environments, *Remote Sensing of Environment*, Vol. 113, No. 8, pp. 1712-1723.

Heinz, D.C. and Chang, C.I. (2001), Fully constrained least squares linear spectral mixture analysis method for material quantification in hyperspectral imagery, *IEEE Transactions on Geoscience and Remote Sensing*, Vol. 39, No. 3, pp. 529-545.

Keshava, N. (2003), A survey of spectral unmixing algorithms. *Lincoln Laboratory Journal*, Vol. 14, No. 1, pp. 55-78.

Lee, D.D. and Seung, H.S. (1999), Learning the parts of objects by non-negative matrix factorization, *Nature*, Vol. 401, No. 6755, pp. 788-791.

Nascimento, J.M.P. and Bioucas-Dias, J.M. (2005),

Vertex component analysis: a fast algorithm to unmix hyperspectral data, *IEEE Transactions on Geoscience and Remote Sensing*, Vol. 43 No. 4, pp. 898-910.

Paatero, P. and Tapper, U. (1994), Positive matrix factorization: a non-negative factor model with optimal utilization of error estimates of data values, *Environmetrics*, Vol. 5, No. 2, pp. 111-126.

Raksuntorn, N. and Du, Q. (2010), Nonlinear spectral mixture analysis for hyperspectral imagery in an unknown environment, *IEEE Geoscience and Remote Sensing Letters*, Vol. 7, No. 4, pp. 836-840.

Röder, A., Kuemmerle, T., and Hill, J. (2005), Extension of retrospective datasets using multiple sensors. an approach to radiometric intercalibration of Landsat TM and MSS data, *Remote Sensing of Environment*, Vol. 95, No. 2, pp. 195-210.

Song, C. (2004), Cross-sensor calibration between Ikonos and Landsat ETM+ for spectral mixture analysis, *IEEE Geoscience and Remote Sensing Letters*, Vol. 1, No. 4, pp. 272-276.

Stathaki, T. (2008), *Image Fusion: Algorithms and Applications* 1st Edition, Academic Press, New York, N.Y.

Teillet, P.M., Fedosejevs, G., Thome, K.J., and Barker, J.L. (2007), Impacts of spectral band difference effects on radiometric cross-calibration between satellite sensors in the solar-reflective spectral domain, *Remote Sensing of Environment*, Vol. 110, No. 3, pp. 393-409.

Yokoya, N., Mayumi, N., and Iwasaki, A. (2013), Cross-calibration for data fusion of EO-1/Hyperion and Terra/ASTER, *IEEE Journal of Selected Topics in Applied Earth Observations and Remote Sensing*, Vol. 6, No. 2, pp. 419-426.

Yokoya, N., Yairi, T., and Iwasaki, A. (2012), Coupled nonnegative matrix factorization unmixing for hyperspectral and multispectral data fusion, *IEEE Transactions on Geoscience and Remote Sensing*, Vol. 50, No. 2, pp. 528-537.